ChemPubSoc Europe

DOI: 10.1002/open.201700131

Open Access ChemistryOPEN Full Papers

A Small Molecule Impedes Insulin Fibrillation: Another New Role of Phenothiazine Derivatives

Meghomukta Mukherjee, Jagannath Jana, and Subhrangsu Chatterjee[a]

Protein misfolding is interrelated to several diseases, including neurodegenerative diseases and type II diabetes. Misfolded/unfolded proteins produce soluble oligomers that accumulate into "amyloid plaques". Inhibition of amyloid-plaque formation by those misfolded/unfolded proteins will lead to the invention of new therapeutic approaches for amyloid-related diseases. Herein, methylene blue (MB), a well-defined drug against multiple diseases and disorders, is used to impede insulin fibrillation. In this study, we perform an array of in vitro experiments to monitor the effects of MB on the fibrillation of bovine insulin. Our results confirm that MB distresses the kinetics of insulin fibrillation by interacting with insulin in its monomeric form. A thioflavin T assay indicates that insulin fibrillation is interrupted upon the addition of MB. The same results are confirmed by circular dichroism, dynamic light scattering (DLS), and size-exclusion chromatography (SEC). According to the DLS data, the insulin fibrils are 800 nm in diameter, and the addition of MB reduces the size of the fibrils, which remain 23 nm in size, and this indicates that no fibrillation of insulin occurs in the presence of MB. This data is also supported by SEC. Saturation transfer difference NMR spectroscopy and molecular dynamics simulations demonstrate the interactions between insulin and MB at the atomic level.

1. Introduction

One of the fundamental processes associated with post-transcriptional modification is protein folding. During this phase of protein modification, numerous proteins undergo misfolding or partial unfolding.[1] These unfolded or misfolded proteins then become responsible for diverse types of diseases and disorders, such as Alzheimer's disease, Huntington disease, Parkinson's disease, and transmission spongiform encephalopathy.[2–6] Mainly, these misfolded proteins are rich in β-sheet structures and are insoluble in most solvents of a physicochemical nature.[7,8]These proteins tend to aggregate into amyloids or amorphous-like structures, which further involves cellular damage and organ dysfunction.[9] The principle behind the development of amyloid fibrils is linked to several steps, such as dissociation or association of protein native structures that further form seeds for nucleation, elongation of the fibrillar aggregates, and finally the formation of larger fibrils or large aggregates such as floccules and tangles.[10–13] Nevertheless, the present understandings of the inhibition of amyloid fibrils remain unsolved.

Insulin can cause type II diabetes if defects occur in insulin metabolism.[14] There is also a great role played by insulin in the formation of "amyloidoma" at the site of injection of the patient taking insulin intravenously. In those cases, insulin starts to deposit in large amounts and forms an amyloidoma, which is pathogenic.[15] Likewise, this aggregation of insulin has had a great effect on drug discovery.[16] Insulin, a 51-residue protein, undergoes partial unfolding or misfolding in vitro.[17] Insulin is a hexameric protein under physiological conditions, and it binds with two or four Zn^{+} ions.[17] Monomeric insulin consists of one A chain of 21 residues and one B chain of 30 residues.[18] The aggregation of insulin mainly comprises noncovalent interactions. During aggregation, the disulfide bonds present in the insulin monomer remain unchanged, so they provide a substantial topological limitation, which thus results in twisting of the A chain.[19,20] Upon heating and under acidic conditions, insulin starts to misfold and forms amyloid assemblies.[21] Bovine insulin differs from human insulin by only three amino acids (A8 Ala-Bov/Thr-Hum, A10 Val-Bov/ Ile-Hum, and B30 Ala-Bov/Thr-Hu), and it also aggregates more easily in vitro, so it shows better results as a model to study protein aggregation.[22] Several experimental studies on insulin indicate that the N and C termini of the B chain play crucial roles during the fibrillation process.[23] The characteristics of the fibrils formed by insulin are analogous to those of other amyloids with similar X-ray diffraction configurations and rich in β-sheet structures, and these fibrils show affinity towards thioflavin T and Congo red dyes, which are highly stable at high tem-

[a] M. Mukherjee, J. Jana, Dr. S. Chatterjee
Department of Biophysics
Bose Institute
P 1/12 CIT, Scheme VII M
Kankurgachi, Kolkata 700054 (India)
E-mail: subhro_c@jcbose.ac.in

Supporting Information and the ORCID identification number(s) for the author(s) of this article can be found under: https://doi.org/10.1002/open.201700131.

peratures and to proteases.[24–27] In a recent study, it was also shown that fibrils could be detected by probing the protein with biphenyl-group-grafted polyamido amine (PAMAM).[28] The exact reasons behind this insulin fibrillation and its inhibition are still to be settled.[29,30] From this point of view, the reason behind deliberately improving the experimental and theoretical conclusions to resolve this cause and to produce the appropriate drug is linked to the numerous steps of insulin aggregation.

A few experimental studies have outlined the inhibition of tau phosphorylation[31] and scrapie formation of prion by phenothiazine compounds.[32] Methylene blue (MB) is a phenothiazine derivative and a cationic dye with the chemical name tetramethylthionine chloride, and it was already shown to have druglike behavior in treating malaria,[33] frontotemporal dementias,[34] and several bacterial and viral infections.[35] Precisely, it is the first synthetic compound used as a drug therapeutically.[36] Also, MB and its derivatives were used in chemotherapy before the discovery of related drugs.[37] In recent times, the potency of MB to suppress cognitive decline in Alzheimer's disease (AD) patients was shown.[38,39] Necula et al. performed biochemical studies and showed that MB inhibited Aβ42 oligomerization with a moderate inhibitory concentration (IC_{50}) value of 12.4 mM in vitro,[40] whereas Taniguchi et al. reported an IC_{50} value of 2.3 mM for the same reaction.[41] In a dose-dependent manner, MB shows its inhibition effects on Aβ42 aggregation. In-depth analysis also revealed that the oligomerization process of the Aβ42 oligomers was converted into a fibrillation process after the addition of MB.[40] To the best of our knowledge, the function of MB in inhibiting the insulin fibrillation process has not been reported.

In this study, we show that MB interacts with insulin monomers and inhibits its fibrillation process. At different concentrations of MB with the insulin monomers, we observed that the highest concentration of MB used was the superlative concentration to inhibit the fibrillation process. All experiments were performed at two different pH values (pH 2.6 and 7.2). The reason behind the two different pH values was to confirm whether MB acted the same at different pH values. Our physiological conditions were neutral, in that determining how MB worked was one of our aims. We confirmed the inhibition action by performing several in vitro experiments. Our first experiment was a thioflavin T assay, by which we found that upon heating and incubating insulin—MB at pH 2.6 for 24 h and insulin—MB at pH 7.2 for 42 h, no fibrils were formed in the insulin–MB complexes. The same conditions were maintained for performing circular dichroism (CD) experiments, and here also, we learned that insulin without MB formed fibrils and showed a β-sheet structure, whereas the α-helical structure of insulin remained the same in the presence of MB. Scanning electron microscopy (SEM), isothermal titration calorimetry, and size-exclusion chromatography (SEC) were performed to determine the mechanism behind the interaction of MB with the insulin monomers. We treated cells with insulin–MB fibrillated samples to determine the inhibition effect of MB on insulin fibrillation. Further, saturation transfer difference (STD) NMR spectroscopy (NMR and T_1, T_2 relaxation) in conjunction with molecular dynamics simulations were employed to observe the atom-specific interaction of MB with insulin.

2. Results and Discussion

2.1. Fibrillation Study by the Thioflavin T Assay

Thioflavin T (ThT) dye is highly sensitive to the construction of fibrils. ThT dye interacts with amyloid fibrils without changing the structure or sequence of the proteins.[42] The dye has emission and excitation bands at $\lambda = 480$ nm and 440 nm, respectively. The mechanism by which ThT dye indicates amyloid fibrils is that the ThT dye binds with the fibrils as fibrillation occurs, and its emission intensity steadily increases. In this study, we performed time-dependent analysis of insulin fibrillation to identify the lag time, and we also measured the utilization of the small molecule. We observed that if the insulin (50 μM) monomers were independently heated, they started to show an increase in the emission spectrum after 11 h in citrate phosphate buffer pH 2.6 and after 20 h in sodium phosphate buffer pH 7.2 (Figures 1a and 2a). After 17 and 37 h of heating incubation, the fibrillation process gradually started to saturate for insulin at pH values of 2.6 and 7.2, respectively. We obtained a sigmoidal curve, from which we concluded the phases of the fibrillation process. This sigmoidal curve represented a three-phase process: log, lag, and static phases, similar to the bacterial growth curve pattern. We obtained the lag or nucleation phase, the elongation or log phase, and the saturating phase. From this curve, we concluded that the nucleation process of insulin fibrillation was sustained up to 11 h, after which it entered the elongation process and continued for another 6 h; then, it finally entered the saturation phase at 17 h (at pH 2.6). From 11 to 17 h there was a maximum increase in the emission spectrum of ThT, which could be the exponential phase, and the duration of this saturation was the static phase for the entire fibrillation process (shown in Figure 1a). Correspondingly, at pH 7.2, we found that for insulin in the absence of MB the lag phase was up to 20 h; this was followed by gradual entering of the exponential phase, which continued for 37 h. After that was the saturation phase. We added the MB during insulin fibrillation process in a mean of concentration approach. MB was used at different concentrations (1:50, 1:100, and 1:500 ratios). At an insulin/MB concentration ratio of 1:50, insulin fibrillation showed a lag phase at 16 h at pH 2.6, and the emission was less intense than the emission for free insulin fibrillation. At this 1:50 ratio, we postulate that MB may interact with a few insulin monomers due to the low concentration of MB, so the emission intensity cannot reach the emission intensity of the free insulin fibrils. At an insulin/MB concentration of 1:100, the effect was more apparent than the effect observed as a 1:50 ratio. An insulin/MB concentration of 1:500 worked the best. No fibrillation was observed even after 24 h of incubation at pH 2.6. This comparative study is shown in Figure 1a. The complexes with 1:50 and 1:100 ratios of insulin/MB enter the exponential phase after 28 and 32 h at pH 7.2, respectively (Figure 2a). However, as previously said for pH 2.6, the intensities of these two 1:50 and 1:100 MB–insulin com-

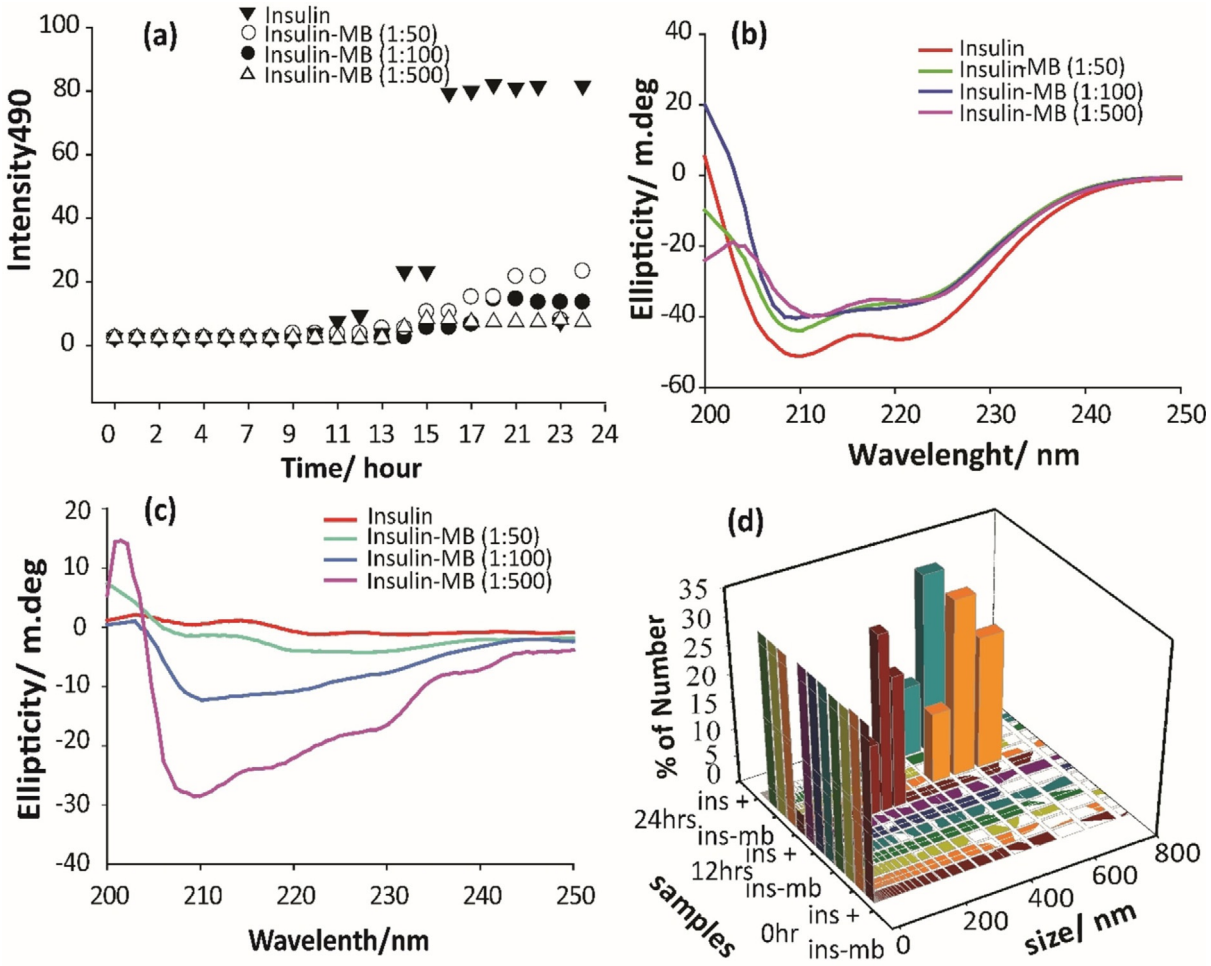

Figure 1. a) ThT assay of insulin with and without MB prepared in citrate phosphate buffer pH 2.6. b) CD spectra of insulin in the presence and absence of MB after 0 min and c) after 24 h. d) DLS data of insulin in the presence and absence of MB. The results of a total of 12 samples are shown in the DLS graph. The samples from right to left or 0 to 24 h are: 0 h (insulin; insulin/MB = 1:50, 1:100, and 1:500), 12 h (insulin; insulin/MB = 1:50, 1:100, and 1:500), and 24 h (insulin; insulin/MB = 1:50, 1:100, and 1:500). All samples were prepared in citrate phosphate buffer pH 2.6.

plexes are much lower than that of insulin alone. The complex with insulin/MB = 1:500 showed no increase in the intensity, even after incubating for 42 h (Figure 2a). The fluorescence of MB was also measured at $\lambda = 450$ to 480 nm, and no increase in the fluorescence intensity was observed. Thus, we can say that the increase in the intensity of insulin in the presence of MB is a result of the inhibition effects of MB towards fibrillation. MB was always added to the initial state before incubation was started.

2.2. Circular Dichroism Spectroscopy as a Means To Reveal Structural Characteristics

Insulin is a globular protein that includes three α helices. During the fibrillation process, several kinds of conformational changes occur in the insulin structure. Insulin forms either an amyloid-like structure or amorphous aggregates at the stage preceding fibrillation. These amyloid fibrils are rich in β-sheet conformations. Hence, if a normal protein undergoes the fibrillation process, a phase transition of the α helix towards a β-sheet conformation emerges. In our study, a freshly prepared insulin sample was incubated in the presence and absence of MB at 50 °C for 24 h for insulin–MB pH 2.6 and for 42 h for insulin–MB pH 7.2, and all the spectra were taken at different time intervals. We also used a different concentration of MB to determine the optimum concentration at which it blocked insulin fibrillation. We observed that free insulin in its initial state (before heating) adopted an α-helical conformation, which was apparent from the presence of two negative ellipses at $\lambda = 208$ and 222 nm. As the free insulin increased in size due to fibrillation at 50 °C, its negative ellipticity gradually decreased with time. The ellipticity decreased from −48 to −4 mdeg (Figure 1b,c) at pH 2.6 and from −29 to −8 mdeg at pH 7.2. Interestingly, insulin, in the presence of MB (1:500) at pH 2.6 and pH 7.2 at 50 °C retained its conformation even after 24 and 42 h of heating incubation, respectively (Figures 1b,c and 2b,c).

At insulin/MB ratios of 1:50 and 1:100, we noticed that after 24 h of incubation, the ellipticity decreased by 20 mdeg, but at pH 7.2, there was no such change in the ellipticity. In conclusion, we can say that at these two concentration ratios of insulin/MB, secondary structures other than the α helices were

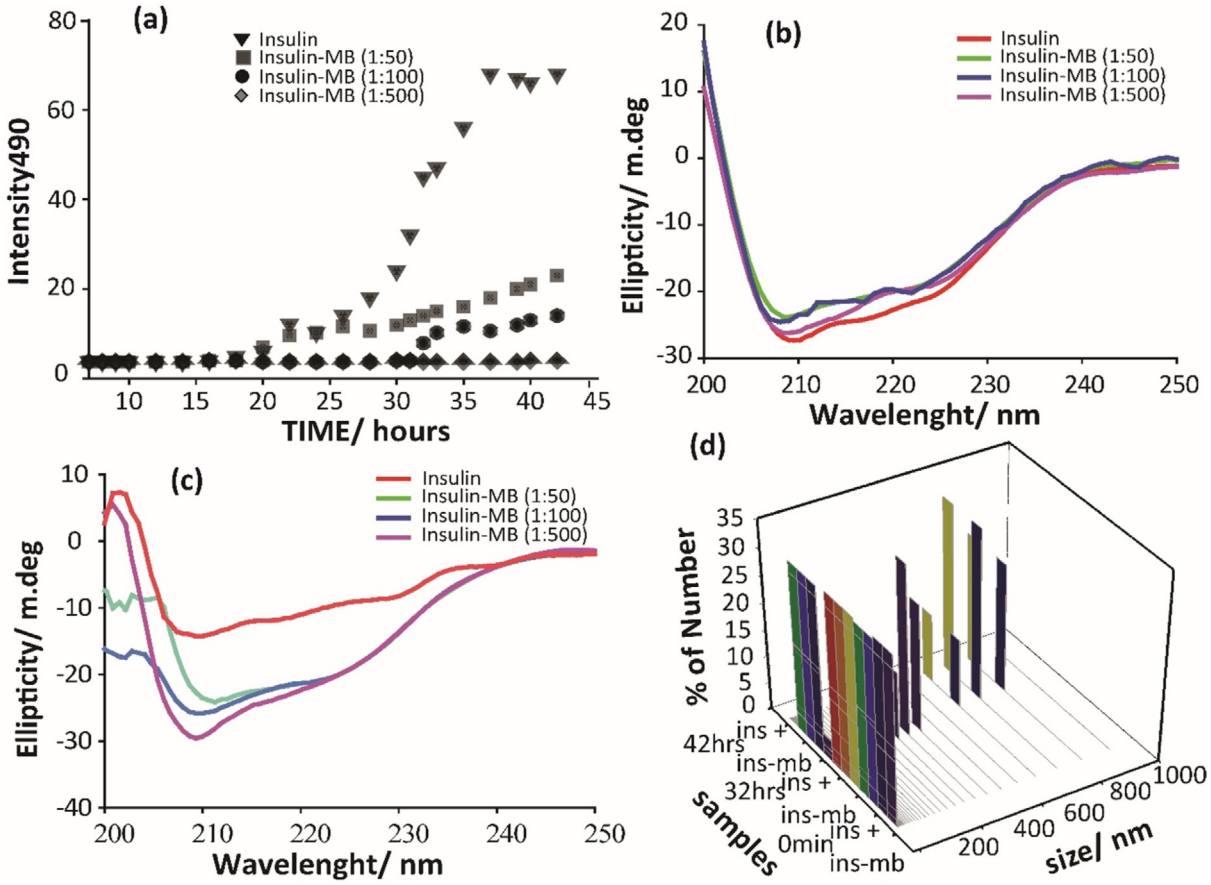

Figure 2. a) ThT assay of insulin with and without MB prepared in sodium phosphate buffer pH 7.2. b) CD spectra of insulin in the presence and absence of MB after 0 min and c) after 24 h. d) DLS data of insulin in the presence and absence of MB. The samples from right to left or 0 to 24 h are: 0 h (insulin; insulin/MB = 1:50, 1:100, and 1:500), 12 h (insulin; insulin/MB = 1:50, 1:100, and 1:500), and 24 h (insulin; insulin/MB = 1:50, 1:100, and 1:500). All the samples were prepared in sodium phosphate buffer pH 7.2.

formed after 24 and 42 h of incubation. To analyze the percentages of helices, β sheets, and random coils, we deconvoluted the raw data by using CDNN software (Table S3 a–d in the Supporting Information). From this analysis, we learned that the helicity of free insulin at pH 2.6 decreased from 61 to 12%, whereas increases in β sheets (18 to 37%) and random coils (17 to 57%) were observed. In the MB–insulin complex, no substantial change in the overall secondary structure of insulin was observed relative to that of free insulin, even after 24 h of incubation. The percentages of helices, β sheets, and random coils were slightly different from the percentages of the t = 0 min conformations. The changes were from 52 to 45% for insulin/MB = 1:50, 52 to 45% for insulin/MB = 1:100, and 48 to 48% for insulin/MB = 1:500 for the α helices. Similar changes in the β sheets and random coils were also observed (Table S3a, b). The CDNN results for pH 7.2 are listed in Table S3c, d. These results indicate that MB binds with the insulin monomers and changes its conformation, as the epitopes for aggregation may remain in buried conformations. By interacting with the insulin monomers, MB inhibits insulin oligomerization. After comparing our CD experimental results with the results obtained by Wang et al.,[42] Kachooei et al.,[43] and Banerjee et al.,[44] we found that MB retained the secondary structure of insulin with more efficiency.

2.3. Increasing the Size of the Oligomer as Studied by Dynamic Light Scattering

After circular dichroism analysis, by which we delineated the changes in the secondary structure of insulin, we wanted to investigate the effect of changing the size of insulin by dynamic light scattering (DLS). In DLS, light is scattered due to the presence of protein aggregates or any noise. The DLS experiment showed that the hydrodynamic radius of insulin in the presence and absence of MB after incubating for 11 h was 0.5 and 50 nm, respectively. Increasing the incubation time of insulin resulted in a larger radius. In the initial state, however, there was no fibrillation, and thus, in the presence of MB the hydrodynamic radius of insulin remained almost the same. As the time increased and fibrillation started, the hydrodynamic radius also increased. At 12 h, the insulin samples were measured, and they gave a diameter of 1 μM, but after 12 h the size increased so much that further measurements were not possible and errors appeared. On the other side, the radius of insulin in the presence of MB (at ratios of 1:50 and 1:100) was measured up to 20 h. After 20 h, the size increased, so no further measurement was possible. For insulin with MB (1:500), no such increase in size was observed, even after 24 h of incubation (Figure 1 d). Only 0.1% of the total population showed

a large size, but 99% of the total population showed no increase in size. During the total time of the measurement, the diameter of the insulin sample remained within 20 to 40 nm. On the other hand, at pH 7.2, the results were almost similar to those obtained at pH 2.6, and insulin/MB = 1:500 worked the best. Here, the insulin lag phase started at 24 h and exponential phase lasted for 32 h, so the measurement was done up to 32 h for insulin in the absence of MB (Figure 2d). However, after 42 h there was no such increase in the dynamic radius of insulin in the presence of MB (1:500).

2.4. Size-Exclusion Chromatography Strongly Supports DLS Results

Size-exclusion chromatography was performed to confirm whether the insulin monomers were binding with the small molecule or not. As insulin stays in the monomeric state, the elution peak came at 42 mL of the total volume of the column. However, upon loading the insulin fibril in the column, the elution peak came at 12 mL. The insulin molecule treated with the small molecule also shown a peak at 42 mL of the eluted buffer, which was very similar to the insulin monomer (shown in Table S1). The principle behind electrophoresis is that larger sized molecules will move faster than smaller sized molecules. Due to higher mass, the large molecular aggregates run fast, and small molecular aggregates run much more slowly. If insulin was not heated, it remained in the monomer state, which was only 5.8 kD in mass, so it eluted last at 42 mL. If the insulin molecule was heated, it formed fibrils, which are large. These large-sized insulin fibrils then acquired higher mobility and ran fast, so they eluted in the very first session of column chromatography. The spectra of the 42 mL eluted sample of the insulin monomer and insulin treated with the small molecule were similar; they both showed peaks at 276 and 238 nm, which are specific to insulin monomers. On the contrary, the insulin fibrils did not retain a band at 276 or 238 nm. The spectrum of the insulin fibrils was flat. The figure is shown in Figure 3. Previous studies on the inhibition of insulin fibrillation revealed that monomeric insulin eluted at last, but as the fibril structure grew, it eluted at the beginning.[45–47] As we already showed by using dynamic light scattering and the thioflavin T assay that the fibrillation process is repressed in the presence of the small molecule, by size-exclusion chromatography we can now validate that if the insulin monomers are treated with the small molecule its fibrillation process is blocked.

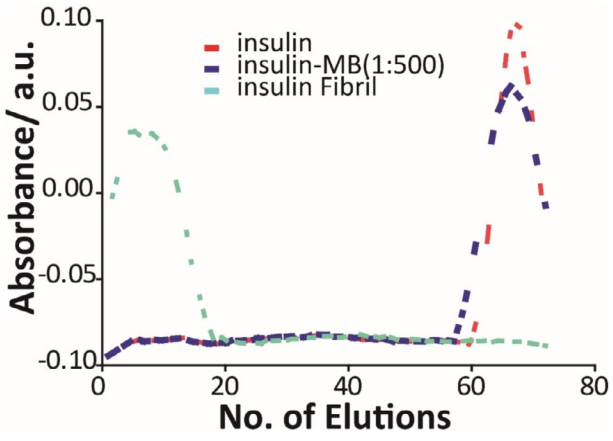

Figure 3. SEC graph obtained for the number of elutions and their absorbance.

2.5. Thermodynamics of Binding as Exemplified by Isothermal Titration Calorimetry

Another important experiment to detect the binding energy of the receptor–ligand interaction is isothermal titration calorimetry (ITC). The change in enthalpy resulting from binding of two different charged molecules was measured by ITC. To see the thermodynamics of binding between the insulin–MB complex, we performed an ITC experiment at 25 °C, and 80 μM insulin was titrated with 2.5 mM MB in citrate phosphate buffer at pH 2.6 and with sodium phosphate buffer at pH 7.2. The titration curves were fitted to a one-site binding model at pH 2.6 and to a three-site binding model at pH 7.2, as shown in Figure 4a,b. The binding of MB with the insulin monomer is a thermodynamically favorable process. The binding of MB with insulin is weak with a binding constant (K_a) value of 1.43×10^3 M^{-1} at pH 2.6 and values of 2.9×10^3, 2.3×10^{-4}, and 7.57×10^{-3} M^{-1} at pH 7.2. Similar findings were previously found by different group with triblocker-PEG, and it was shown that chitosan could bind with both human and bovine insulin with moderate binding energies and K_a values. Calculation of the free binding energy for the insulin inhibitory reaction was not reported. The enthalpy, free binding energy, and entropy are listed in Table S2a,b. The free binding energy calculated from the raw data was -5.230 kcal M^{-1} at pH 2.6 and 4.7, 5.7, and -5.3 kcal M^{-1} at pH 7.2. The reaction process is an apparently exothermic one. All the graphs are shown in Figure 4a,b. All the thermodynamic parameters, free energy change (ΔG), enthalpy change (ΔH), and entropy change (ΔS), were found to be negative, which demonstrates that the entropy of the solvent molecules released from the site of binding is highly positive, whereas the atomic motion of the receptor as well as that of the ligand is reduced to a large extent because of the formation of a hydrogen bond between insulin and MB; this dictates a decrease in the enthalpy of the whole complex. The resultant effect of enthalpy and entropy results in a negative ΔG value for complexation.

2.6. Morphological Study of the Fibrils by Scanning Electron Microscopy and Confocal Microscopy

To confirm the contribution of MB to inhibition of insulin fibrillation, we used scanning electron microscopy (SEM) and confocal microscopy. All samples of insulin and MB at pH 2.6 and pH 7.2 were incubated for 24 and 42 h at 50 °C (insulin/MB = 1:500), and none of the samples showed fibril-like morphology. However, at insulin/MB ratios of 1:50 and 1:100, some amorphous aggregates were found. To validate this insulin morphology, we also performed confocal electron microscopy. Insulin incubated without MB showed a fibril structure, as observed

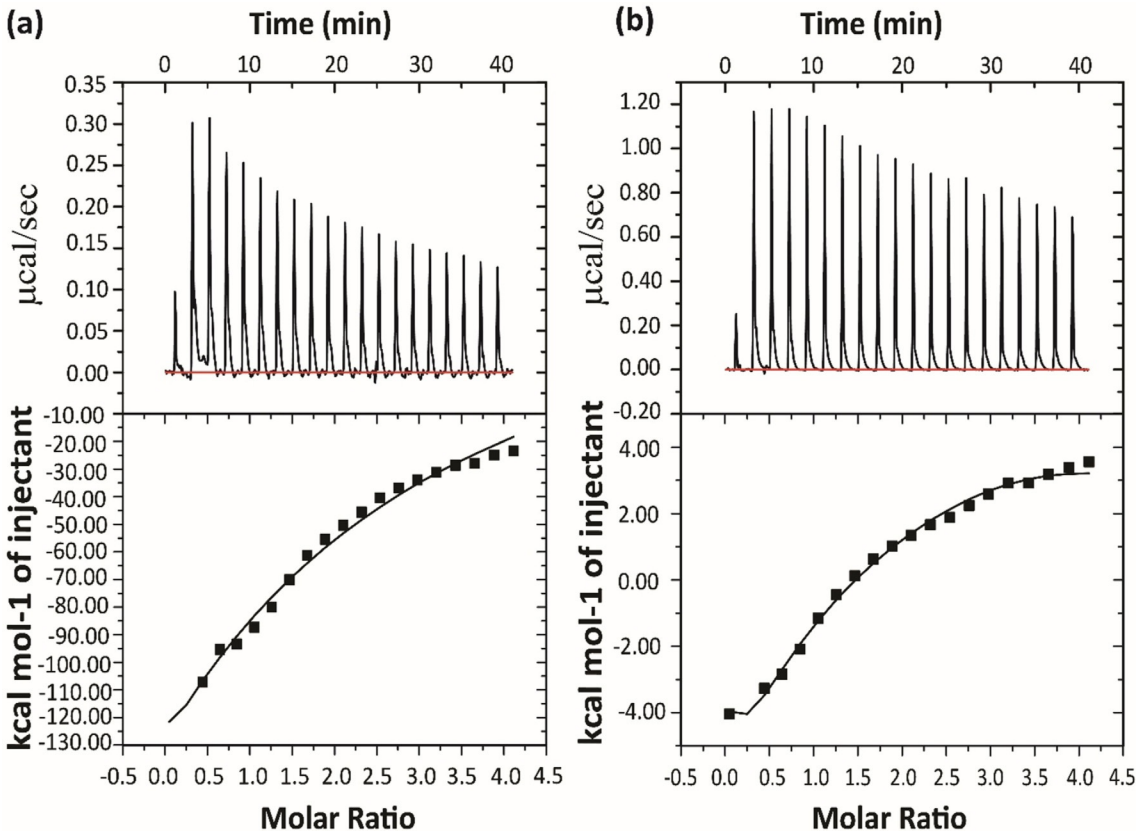

Figure 4. ITC graph of a) insulin and MB, pH 2.6 and b) insulin and MB, pH 7.2. All experiments were performed at room temperature, and this graph was obtained after subtracting the buffer.

by SEM, but if it was incubated with MB (insulin/MB = 1:500), no such fibrillar structure was found (Figure 5a, b). From this incubated sample, an aliquot of 10 µL was kept aside to prepare a sample for confocal microscopy. The confocal microscopy results demonstrated that the insulin sample without MB had a fibril nature, and in the presence of MB there was no fibrillar morphology (Figure 6).

2.7. Atomic-Level Study by using STD-NMR Spectroscopy and T_1/T_2 Relaxation NMR Spectroscopy

STD NMR spectroscopy is an indispensable technique to unravel the key residues of a ligand that interact with the receptor at atomic resolution. A one-dimensional STD NMR spectroscopy experiment was performed to identify the important protons of MB that interact with insulin. In the STD NMR spectroscopy experiment, an excess amount of the ligand (≈100-fold molar excess) relative to its receptor was used with a dissociation constant in the low micromolar to millimolar range. The STD signal was produced by effective magnetization transfer from the receptor to the ligand in its bound state. STD NMR spectroscopy provided us with the binding site or epitope for MB, which is shown in Figure 8a. From the STD-NMR spectroscopy experiment, we can say that the 1-CH, 2-CH, 3-CH, and 4-CH protons of the aromatic ring interact with the insulin monomers and that the 1-CH_3 group also interacts with insulin. The PyMOL structure of MB with the protons marked is shown in Figure 8b. To reveal the atomic-level dynamics of MB and the MB–insulin complex, one-dimensional longitudinal ($R_1 = 1/T_1$) and transverse relaxation ($R_2 = 1/T_2$) experiments were performed. The longitudinal relaxation rate (R_1) of the MB–insulin complex was significantly lower than that of free MB for all amide protons (Figure 8c, d). The rate of longitudinal relaxation is proportional to the correlation time (τ_c). The conformational dynamics of free MB are restricted in the presence of insulin. The decrease in the correlation time is reflected in a reduction in the rate of longitudinal relaxation. Similarly, the transverse relaxation rate (R_2) for all the residues of MB was increased in the presence of insulin.

2.8. Insulin Pathway Study By Treating HepG2 Cells with Insulin in the Presence and Absence of MB

Cells were treated with fibrillated insulin prepared with or without the different molar ratios of MB, and phosphorylation of Akt at Ser473 in the whole-cell lysates was analyzed as a readout for insulin signaling. Our results show that phosphorylation of Akt was enhanced upon increasing the concentration of MB with a maximal effect at insulin/MB = 1:500. These data suggest that dose-dependent inhibition of insulin fibrillation by MB also improved cellular insulin sensitivity (Figure 7).

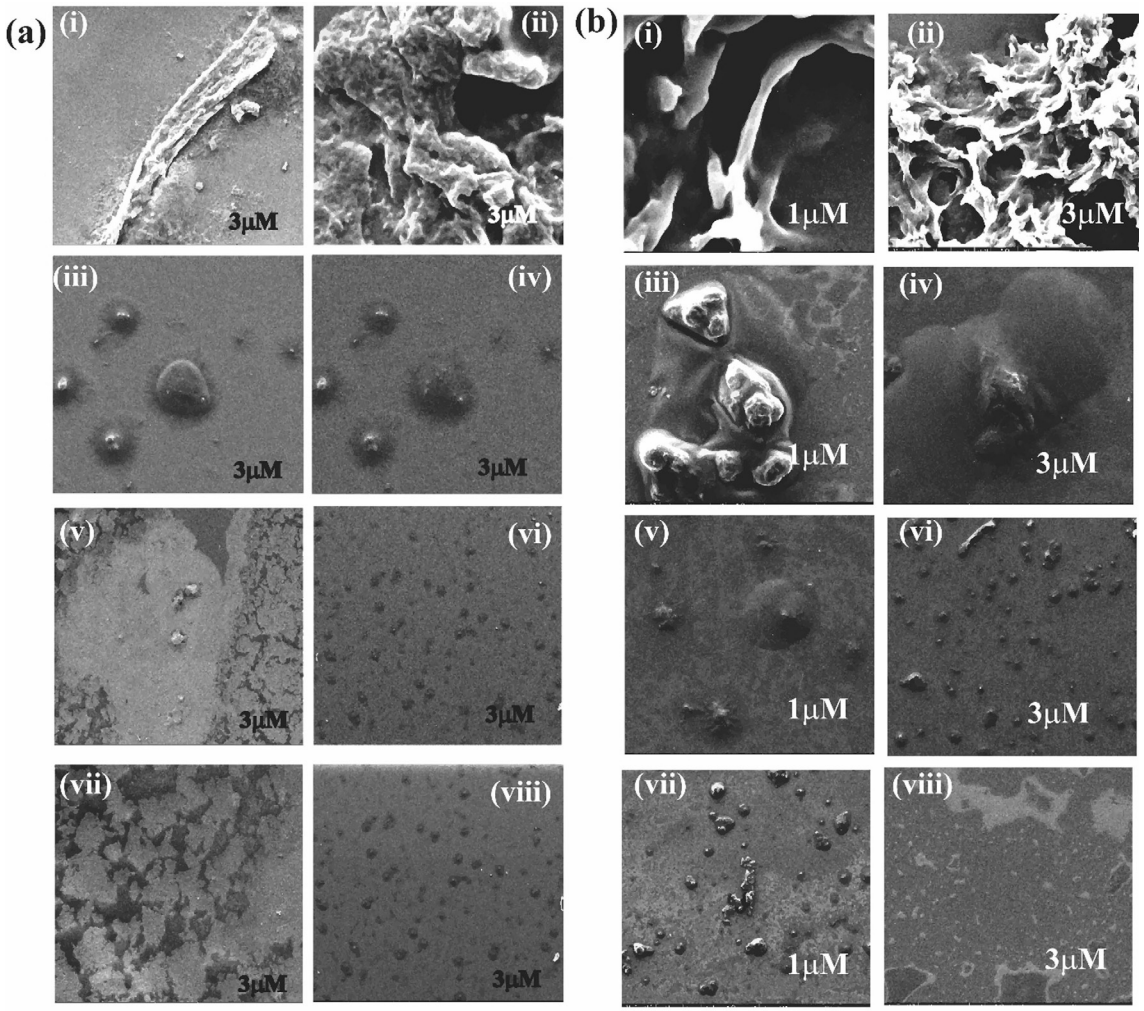

Figure 5. SEM images of a) samples prepared in citrate phosphate buffer pH 2.6 and incubated for 24 h and b) samples prepared in sodium phosphate buffer pH 7.2 and incubated for 42 h. i, ii) insulin alone, iii, iv) insulin/MB = 1:50, v, vi) insulin/MB = 1:100, and vii, viii) insulin/MB = 1:500.

2.9. Molecular Dynamics Simulation Provides Atomic Level and Structural Analysis

A molecular dynamics (MD) simulation showed insight into the mechanism of binding in the MB–insulin interaction. In our dynamics part, residues 1 to 21 are from chain A and residues 22 to 51 are from chain B of the insulin monomer. During this total simulation run, we observed that MB interacted with insulin mainly through the hydrogen atoms of the phenol rings. The interactions were mostly hydrogen bonds and van der Waals interactions; all are shown in Figure S1 a. These interactions between MB and insulin were also found by STD-NMR spectroscopy. The MD simulation gave detailed information about complex formation at the atomic level.[48,44] In its mean individual solvent, molecule MB adjusts its position with regard to the initial docked state.[49] The binding ratio obtained from ITC was found to be 1:1 for the insulin–MB complex at pH 2.6. Hence, we docked MB and insulin up to a 1:1 ratio. To gain more information at the atomic level, the MD simulation was performed for 100 ns for the insulin control and for the 1:1 insulin–MB complex. The average structures of the insulin control obtained from the MD simulation were superimposed in the final 100 ns of the trajectory at intervals of 10 ns (Figure S2). Similarly, the average structures of the insulin–MB complex were superimposed in the final 100 ns of the MD simulation (Figure S3). We determined conformational maintenance and distinctions on the basis of the root-mean-square deviation (RMSD) values. A high RMSD value indicates a flexible nature of the protein, which causes overall instability of the protein's secondary structure.[50] Cpptraj script were incorporated to calculate the RMSD values.[51] The equation used to calculate the RMSD values is [Eq. (1)]:

$$\mathrm{RMSD} = \sqrt{\frac{1}{N}\sum_{i=1}^{N}\delta_i^2} \qquad (1)$$

in which N is the total number of atoms under consideration and δ is the distance between the two positions of N pair of equivalent atoms. Figure 8 e shows the RMSD plot of the insulin control and the 1:1 insulin–MB complex over the simulation timescale. The stability of the trajectories of the complex can be observed with minimal fluctuation ranging from 2 to 2.8 Å.

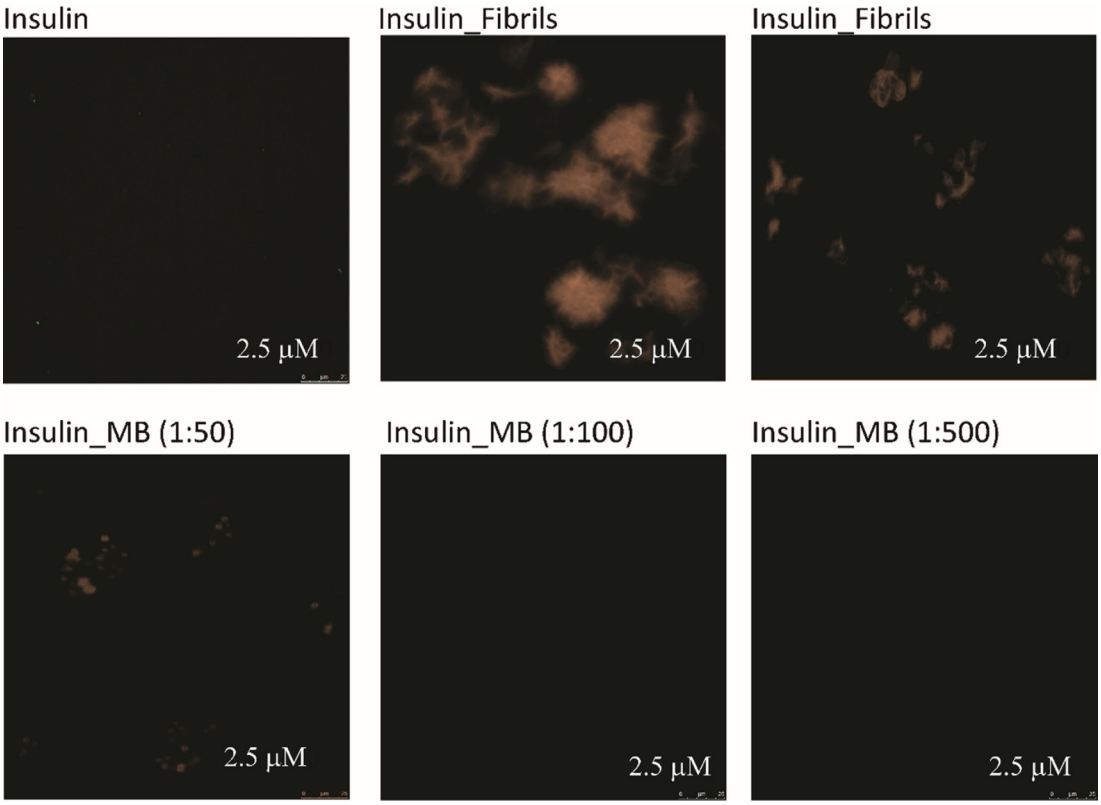

Figure 6. Confocal image of insulin in the presence and absence of MB in concentration ratios of 1:50, 1:100, and 1:500. All samples were prepared at pH 2.6 and incubated for 24 h.

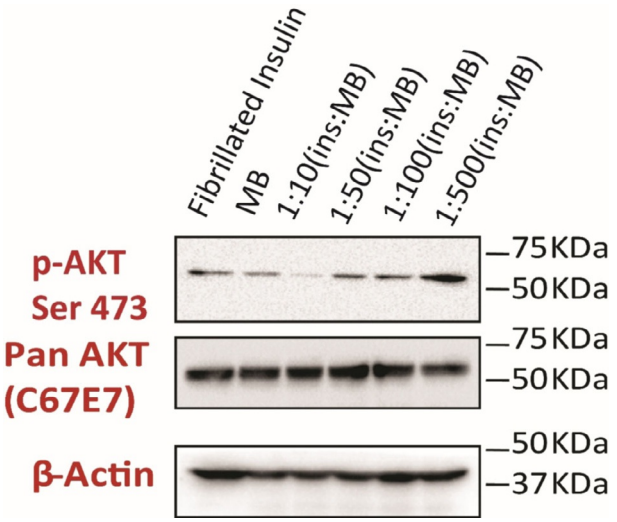

Figure 7. Study of the insulin-signaling pathway.

The RMSD plot of the complex was stable over the entire simulation timescale, from which it could be concluded that MB stabilized insulin. Figure 8 f shows the root-mean-square fluctuation (RMSF) of the insulin control and the insulin–MB complex. In this report, we observed the folding of insulin in the free state and bound with MB and the pattern of MB binding. The RMSD was calculated for a total time of 100 ns (Figure 8 e). During the entire simulation, the MB–insulin complex overcame the lower RMSD trend, whereas free insulin had a higher RMSD value. Also, after 4000 frames the overall RMSD was retained at around 2.0 Å for the insulin complex, but after 4000 frames the RMSD of free insulin was around 2 to 4.0 Å. The RMSD results indicate that free insulin is highly flexible, that is, there is a continuous change in its conformation. This highly flexible state will possibly lead to instability of the insulin monomer, which might be the reason why it forms aggregates. However, the MB–insulin complex with a lower RMSD suggests that MB stabilizes the secondary structure of insulin. The structural stability of insulin resulting from MB might be the reason for the inhibition of insulin aggregation. Therefore, we can approximately propose that inhibition of the fibrillation process of insulin happens if MB interacts with the insulin monomers. Hua et al.[18] illustrated the structural characteristics of insulin on the basis of biophysical analysis, and they found that the N termini of chain A and chain B of the insulin monomer were not in an ordered form during the fibrillation process. Also, the C terminus of chain B forms a B turn under normal conditions; however, during fibrillation this segment forms a helix-like structure.[18] The N-terminal residues of chain A and chain B, which are mainly involved in the aggregation process, are I2, V3, and C6 for chain A and F1, V2, and C6 for chain B. The partial disordered nature of chain A and chain B exposes possible sites of aggregation. The molecular dynamics results also indicate a similar situation in that if MB is in a bound state with insulin, the N-terminal fragment of chain A maintains a structure that is similar to the initial structure of insulin >. However, free

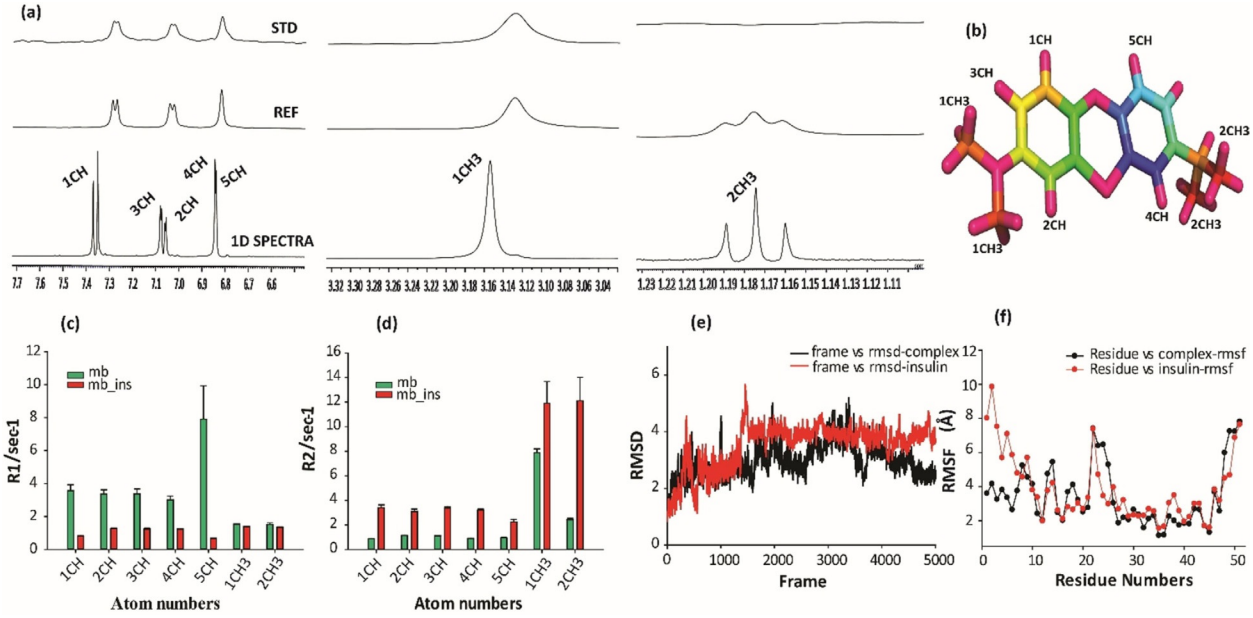

Figure 8. a) STD-NMR spectra of MB in the presence of insulin. b) Image of MB prepared with PyMOL; protons are marked. c, d) T_1 and T_2 relaxation of MB–insulin and insulin, respectively. RMSD and RMSF of e) free insulin and f) the insulin–MB complex.

insulin gives different results and shows that the N-terminal fragments of the A chain are exposed compared to the initial insulin structure (shown in Figure S1 b). The RMSF analysis is illustrated in Figure 8 f, and it can be concluded that chain A (residues 1–21) and chain B (residues 22–51) are less flexible in the insulin–MB complex than in free insulin. However, certain residues of free insulin in chain B (residues 28, 37, 38, 39, and 40) and chain A (residues 1 to 8) show high fluctuation during the simulation runtime. Upon binding of insulin with the peptide, there were no such changes in these residues. Residues 1–8 of chain A have a helix structure, so less fluctuation in these residues in the presence of MB suggests that MB stabilizes the helix of insulin, which is an indication that the fibril-like structure is not formed during the total simulation run. The molecular simulation study offers mechanistic insight into how MB interacts with the insulin monomer.

3. Conclusions

We showed in this report that methylene blue (MB) interacts with insulin monomers in a ratio of 500:1 and displays inhibition effects on the aggregation process of insulin. We used different concentrations of MB to check the inhibition effect, and we found that if the insulin/MB ratio was 1:50 or 1:100 no such fibrillar structure was formed but amorphous aggregates were present. As we increased the concentration of MB, we found that the fibrillation process, as well as the formation of amorphous aggregates, was blocked. Previous experiments performed by Wang et al.[52] and Choudhary et al.[53] were performed with high concentrations of the inhibitors to inhibit insulin fibrillation. Our molecule also worked best at high concentrations. Our hypothesis was supported by various experiments, that is, thioflavin T (ThT) assay, circular dichroism (CD), dynamic light scattering (DLS), size-exclusion chromatography (SEC), scanning electron microscopy (SEM), confocal microscopy, and Akt phosphorylation assay performance. Interaction of MB with the insulin monomers was confirmed by saturation transfer difference (STD) NMR spectroscopy, isothermal titration calorimetry (ITC), and molecular dynamics experiments. From the STD NMR spectroscopy and molecular dynamics experiments, we found that the hydrogen atoms of MB interact with the insulin monomers. The hydrogen atoms of the aromatic ring interact with the insulin monomers. Also, the molecular dynamics and docking results suggested that MB interacts with a helix of the B chain of the insulin monomer. During a total simulation run of the MB–insulin complex, it remained bound with insulin in that particular position. Upon treating the HepG2 cell line with fibrillated insulin in the presence and absence of MB, we observed that the complex with a 1:500 ratio of insulin/MB showed Akt phosphorylation, as MB inhibited fibrillation of insulin, so the concentration of monomeric insulin remained high. By performing the abovementioned experiments, we concluded that the insulin–MB complex was far more stable than free insulin and the dissociation of MB from insulin was also not possible even at high temperatures/acidic pH values as well as at low temperatures. However, it was previously reported that MB inhibited tau phosphorylation[31,41] and also abeta-42,[40] and we further assume that this type of drug can act in both diseases at a single time. MB has shown diverse potential in impeding protein aggregation and proves to be a lead for developing better therapeutics.

Experimental Section

Thioflavin T Assay

Thioflavin T is a dye specific for the detection of protein fibrillation. It has an excitation wavelength at 440 nm and an emission wave-

length at 480 nm. We prepared insulin in citrate phosphate buffer pH 2.6 and sodium phosphate buffer pH 7.2. In both cases, the concentration of insulin was 50 μM. The small molecule was co-incubated with the insulin monomers at the very beginning of the experiments. At several time intervals, data were collected. The small molecule was used at different concentrations, that is, insulin/MB = 1:50, 1:100, and 1:500.

Circular Dichroism (CD)

Secondary structural changes in insulin over time were analyzed by circular dichroism. Insulin is a globular protein that shows a helical structure at $\lambda = 222$ and 208 nm. All spectra were analyzed by a Jasco 815 circular dichroism spectropolarimeter at 25 °C. The final concentration of insulin was 25 μM. The scanning wavelength was from 200 to 260 nm. The speed of each scan was 100 nm s^{-1}, and the bandwidth was 1 nm. The results of each spectrum are averaged over three scans. Buffer's spectra were subtracted from the insulin spectra. All the spectra were measured in a time-dependent manner.

Scanning Electron Microscopy (SEM)

Scanning electron microscopy is a low-resolution instrument that takes images of a molecule's morphology. Insulin samples (50 μM) were incubated with and without MB at 50 °C. From the incubated insulin samples, aliquots (5 μL) were taken for SEM analysis. Samples were coated with gold in an Edward's S150 Sputter Coater before scanning. Finally, images were taken by using an FEI QUANTA 200 scanning electron microscope. Insulin was mixed with MB in ratios of 1:500, 1:100, and 1:50.

Confocal Microscopy

Confocal microscopy is also another microscopy technique that can be used to confirm SEM data. It uses the fluorescence of the molecules to conduct the imaging. For all analyses, a 20× or 40× oil immersion objective was used with a fluorescence microscope (DMRE, Leica, Germany) equipped with one beam splitter (488) and FW TD 488/543/633 beam-splitting excitation mirrors. All samples were prepared as previously described for the SEM experiments. Those samples were spread on a glass slide and covered with a cover slip. The edges were then glued.

Dynamic Light Scattering (DLS)

DLS studies were performed with Malvern nanodynamic light scattering equipment. The insulin sample was taken at a concentration of 50 μM in the presence and absence of MB for analysis. All the samples were filtered through a microfilter with a pore size of 0.2 μM.

The measured size is presented as the average value of 25 runs. Dynamics 7.10.0.10 software at optimized resolution was used for data analysis. The mean of the hydrodynamic radius (R_h) and polydispersity (P_d) was assessed by using the Stokes–Einstein equation [Eq. (2)]:

$$R_h \approx kT = 6pgD250CW \quad (2)$$

in which R_h is the hydrodynamic radius, k is the Boltzmann constant, T is the absolute temperature, g is the viscosity of water, and D25uCw is the translational diffusion coefficient.

Isothermal Titration Calorimetry (ITC)

The ITC experiment was performed at 25 °C with VP ITC Micro Calorimetry equipment. The insulin solution was taken in a cell, MB was taken in a syringe, and the buffer was taken in a reference cell. We experimented with buffers of pH 2.6 and pH 7.2. The insulin solution was stirred at 300 rpm by the syringe. This titration of insulin with MB was performed for a total of 14 injections. The first injection was of 1 μL, which was not assumed in the analysis, and all the remaining injections were 3 μL. The heat of dilution was subtracted from the main titration data. After equilibration was reached, only then was the titration started. All the data were analyzed in origin software. The heat change (ΔG) and the entropy change (ΔS) were calculated from the thermodynamics law equation.

Size-Exclusion Chromatography (SEC)

Size-exclusion chromatography was performed at room temperature with a Biorad torosh column. The insulin was taken in 1 mg mL^{-1}. MB was added in a 1:500 ratio. After 24 h of incubation at 50 °C, the samples were separately run in the column. The total column volume was 50 mL. The void volume of the column was 15 mL. We started to collect the sample after the void volume was released. A total of 50 mL of the sample was collected from the column for each sample.

NMR Spectroscopy (STD NMR, T_1 and T_2 Relaxation)

To perform the STD NMR spectroscopy experiments, we prepared samples in 99.0% D_2O, and the pH was adjusted to 2.6. NMR is a high-resolution spectroscopy technique used to detect structure, dynamics, and interactions between molecules. All NMR spectra were recorded by using a Bruker AVANCE III 500 MHz spectrometer equipped with a 5 mm SMART probe at 298 K. Data acquisition and processing were performed by using Topspin 3.1 software. All NMR samples were prepared in 50 mM citrate phosphate buffer containing 10% D_2O and using trimethylsilylpropanoic acid (TSP) as an internal standard (0.0 ppm). Insulin powder was dissolved in 600 μL citrate phosphate buffer (pH 2.6) with D_2O containing TSP. STD NMR spectroscopy was done for three samples: reference, in the presence of insulin, and in the absence of insulin.[44] Atomic-level dynamics were obtained from one-dimensional longitudinal (T_1) and transverse (T_2) relaxation experiments. The T_1 experiments were performed by using previously reported protocols[54,55] with different inversion recovery delays ranging from 0 to 3 s. The T_2 measurements were achieved from the CPMG sequence with delays ranging from 0 to 0.7 s.

Cell Lines and Culture Conditions

HepG2 cells were cultured in standard Dulbecco's modified Eagle's medium (DMEM) (HiMedia), 10% fetal bovine serum (FBS) (GIBCO). Cells were maintained in a 6 cm dish until confluency. Then, existing media were discarded and replenished with serum-free media for 4 h. After 4 h, cells were treated with fibrillated insulin and different dilutions of the respective small molecule in fibrillated insulin (1:10, 1:50, 1:100, 1:500). After 15 min of treatment, cells were harvested, and samples were prepared for western blotting.

Antibodies and Reagents

The following antibodies and reagents were obtained commercially: anti-phospho Akt (Ser473) antibody (4058, rabbit, Cell Signalling), anti-Akt (pan) antibody (4691, rabbit, Cell Signalling), and anti-α-actin antibody (mouse, Cell Signalling).

Western Blotting

For western blotting, cells were lysed in cell lysis buffer [50 mM Tris-HCl pH 7.2, 100 mM NaCl, 1 mM EDTA (ethylenediaminetetraacetic acid) pH 8.0, 1 mM EGTA (ethylene glycol-bis(2-aminoethylether)-*N*,*N*,*N*′,*N*′-tetraacetic acid), 1% Triton X100] and protease and phosphatase inhibitor tablets (Roche). 10% Resolving gel (1.5 M Tris-HCl, pH 8.8) and 4% stacking gel (0.5 M Tris-HCl, pH 6.8) were cast in a GE Healthcare MiniVe sodium dodecyl sulfate (SDS) electrophoresis system. 10% APS (Himedia #MB003-25G), *N*,*N*,*N*′,*N*′-tetramethylethylenediamine (TEMED) (Sigma #T9281-50ML), and 10% SDS were added to cast the gel. Protein (30–50 μg) was prepared with 5× SDS sample loading dye (10% β-mercaptoethanol) and boiled for 10 min at 95 °C. Then, the sample was kept on ice for 5 min and centrifuged shortly and loaded. Run was performed at 90 V for 10 min and at 120 V for the rest of the duration. The transfer was done in MiniVe transfer apparatus by using a Millipore polyvinylidene difluoride (PVDF) membrane (IPVH000-10). Transfer duration was either overnight at 25 V or 3 h at 90 V at 4 °C, whereas 400 mA was preset. Membranes were kept in 1×PBST [1×phosphate-buffered saline (PBS), 1% Tween20 (Sigma #P1379IL)] for 5 min then in 5% NFDM for 1 h at room temperature. Then, the membranes were washed with 1×PBST (3×), 5 min each time, and incubated in desired primary antibody at 4 °C overnight. After that, the membrane was washed with 1×PBST (3×) and incubated with appropriate secondary antibody for 1 h at RT and then developed by using Millipore Luminata Classico (#WBLUC0500) or Luminata Forte (#WBLUF0100) HRP substrates and picture were captured in Gel Logic Carestream 400PRO.

Docking

Methylene blue was docked with insulin in Glide module by using the standard precision (SP) mode (Glide, version 5.5, Schrodinger, Inc., New York, NY, 2009). The grid was prepared to cover the entire structure of insulin with dimensions of −29×7×40 Å. MB was docked with insulin to obtain a 1:1 complex.

Molecular Dynamics Simulation

MD simulations were performed in Amber14 by using prmbsc0 modifications in conjunction with ff99SB force field for insulin. Parametrization of MB was performed in the simple harmonic function used by General Amber Force Field (GAFF) with AM1-BCC charge model.[56] The insulin–MB complex was already neutralized, so no extra ions were required to neutralize the system. TIP3P water model was used to solvate the system in an octahedral model with edge length extensions of 10 Å from solute atom.[57] The simulation was performed by using periodic boundary conditions with the particle-mesh Edward simulation method.[58] Lennard–Jones potentials and direct space interactions cut-off were 9 Å to correct for long-range van der Waals interactions. The SHAKE algorithm was used to restrain the hydrogen atoms with an integration time step of 2 fs.[59] Energy minimization was performed under explicit solvent conditions. MD simulations were continued up to 100 ns, and the trajectory was collected at an interval of 2 ps for all systems. The trajectory of the MD simulation was analyzed by using the cpptraj module of Amber tools14.[51]

Acknowledgements

We would like to acknowledge Department of Science & Technology (DST) Innovation in Science Pursuit for Inspired Research (INSPIRE), Council of Scientific and Industrial Research (CSIR), ad hoc for financial support. We would like to acknowledge Mr. Souvik Roy for helping in ITC (IPLS, Calcutta University). We would also like to acknowledge Mr. Deepak Chandra Konar and Dr. K.P. Das for providing an instrumental facility for size-exclusion chromatography.

Conflict of Interest

The authors declare no conflict of interest.

Keywords: amyloids · fibrillation · NMR spectroscopy · noncovalent interactions · protein folding

[1] C. M. Dobson, *Nature* **2003**, *426*, 884–890.
[2] a) J. D. Harper, S. S. Wong, C. M. Lieber, P. T. Lansbury, *Chem. Biol.* **1997**, *4*, 119–125; b) J. D. Harper, P. T. Lansbury Jr., *Annu. Rev. Biochem.* **1997**, *66*, 385–407.
[3] L. C. Serpell, J. Berriman, R. Jakes, M. Goedert, R. A. Crowther, *Proc. Natl. Acad. Sci. USA* **2000**, *97*, 4897–4902.
[4] J. D. Sipe, A. S. Cohen, *J. Struct. Biol.* **2000**, *130*, 88–98.
[5] G. S. Jackson, A. R. Clarke, *Curr. Opin. Struct. Biol.* **2000**, *10*, 69–74.
[6] J.-C. Rochet, T. Fleming Outeiro, K. A. Conway, T. T. Ding, M. J. Volles, H. A. Lashuel, R. M. Bieganski, S. L. Lindquist, P. T. Lansbury, *J. Mol. Neurosci.* **2004**, *23*, 23–33.
[7] P. Friedhoff, M. von Bergen, E.-M. Mandelkow, E. Mandelkow, *Biochim. Biophys. Acta, Mol. Basis Dis.* **2000**, *1502*, 122–132.
[8] H. H. Lee, T. S. Choi, S. J. C. Lee, J. W. Lee, J. Park, Y. H. Ko, W. J. Kim, K. Kim, H. I. Kim, *Angew. Chem. Int. Ed.* **2014**, *53*, 7461–7465; *Angew. Chem.* **2014**, *126*, 7591–7595.
[9] V. M. Lee, M. Goedert, J. Q. Trojanowski, *Annu. Rev. Neurosci.* **2001**, *24*, 1121–1159.
[10] M. Manno, E. F. Craparo, A. Podestà, D. Bulone, R. Carrotta, V. Martorana, G. Tiana, P. L. San Biagio, *J. Mol. Biol.* **2007**, *366*, 258–274.
[11] D. M. Walsh, I. Klyubin, J. V. Fadeeva, W. K. Cullen, R. Anwyl, M. S. Wolfe, M. J. Rowan, D. J. Selkoe, *Nature* **2002**, *416*, 535–539.
[12] D. J. Selkoe, *Science* **2002**, *298*, 789–791.
[13] I. Langmuir, D. Waugh, *J. Am. Chem. Soc.* **1940**, *62*, 2771–2793.
[14] B. C. Martin, J. H. Warram, A. Krolewski, J. Soeldner, C. Kahn, R. Bergman, *Lancet* **1992**, *340*, 925–929.
[15] a) D. Grunes, A. Rapkiewicz, A. Simsir, *CytoJournal* **2015**, *12*, 15; b) M. R. Nilsson, *Amyloid* **2016**, *23*, 139–147.
[16] S. G. Albert, J. Obadiah, S. A. Parseghian, M. Y. Hurley, A. D. Mooradian, *Diabetes Res. Clin. Pract.* **2007**, *75*, 374–376.
[17] X. Chang, A. M. M. Jørgensen, P. Bardrum, J. J. Led, *Biochemistry* **1997**, *36*, 9409–9422.
[18] Q.−x. Hua, M. A. Weiss, *J. Biol. Chem.* **2004**, *279*, 21449–21460.
[19] a) N.-T. Yu, C. Liu, D. O'Shea, *J. Mol. Biol.* **1972**, *70*, 117–132; b) N.-T. Yu, C. Liu, *J. Am. Chem. Soc.* **1972**, *94*, 3250–3251.
[20] J. Dong, Z. Wan, M. Popov, P. R. Carey, M. A. Weiss, *J. Mol. Biol.* **2003**, *330*, 431–442.
[21] D. F. Waugh, *J. Am. Chem. Soc.* **1944**, *66*, 663–663.
[22] L. Nielsen, R. Khurana, A. Coats, S. Frokjaer, J. Brange, S. Vyas, V. N. Uversky, A. L. Fink, *Biochemistry* **2001**, *40*, 6036–6046.
[23] J. L. Jiménez, E. J. Nettleton, M. Bouchard, C. V. Robinson, C. M. Dobson, H. R. Saibil, *Proc. Natl. Acad. Sci. USA* **2002**, *99*, 9196–9201.
[24] Y. Porat, A. Abramowitz, E. Gazit, *Chem. Biol. Drug Des.* **2006**, *67*, 27–37.

[25] I. Roterman, M. Król, M. Nowak, L. Konieczny, J. Rybarska, B. Stopa, B. Piekarska, G. Zemanek, *Med. Sci. Monit.* **2001**, *7*, 771 – 784.
[26] R. Khurana, V. N. Uversky, L. Nielsen, A. L. Fink, *J. Biol. Chem.* **2001**, *276*, 22715 – 22721.
[27] C. C. Blake, L. C. Serpell, M. Sunde, O. Sandgren, E. Lundgren, *Nat. Origin Amyloid Fibrils* **1996**, 6 – 21.
[28] Q. Huang, J. Xie, Y. Liu, A. Zhou, J. Li, *Bioconjugate Chem.* **2017**, *28*, 944 – 956.
[29] R. Khurana, C. Ionescu-Zanetti, M. Pope, J. Li, L. Nielson, M. Ramírez-Alvarado, L. Regan, A. L. Fink, S. A. Carter, *Biophys. J.* **2003**, *85*, 1135 – 1144.
[30] R. Jansen, W. Dzwolak, R. Winter, *Biophys. J.* **2005**, *88*, 1344 – 1353.
[31] M. Hattori, E. Sugino, K. Minoura, Y. In, M. Sumida, T. Taniguchi, K. Tomoo, T. Ishida, *Biochem. Biophys. Res. Commun.* **2008**, *374*, 158 – 163.
[32] P. K. Baral, M. Swayampakula, M. K. Rout, N. N. Kav, L. Spyracopoulos, A. Aguzzi, M. N. James, *Structure* **2014**, *22*, 291 – 303.
[33] a) J. L. Vennerstrom, M. T. Makler, C. K. Angerhofer, J. A. Williams, *Antimicrob. Agents Chemother.* **1995**, *39*, 2671 – 2677; b) M. Wainwright, L. Amaral, *Trop. Med. Int. Health* **2005**, *10*, 501 – 511.
[34] a) T. Arai, M. Hasegawa, T. Nonoka, F. Kametani, M. Yamashita, M. Hosokawa, K. Niizato, K. Tsuchiya, Z. Kobayashi, K. Ikeda, *Neuropathology* **2010**, *30*, 170 – 181; b) M. Yamashita, T. Nonaka, T. Arai, F. Kametani, V. L. Buchman, N. Ninkina, S. O. Bachurin, H. Akiyama, M. Goedert, M. Hasegawa, *FEBS Lett.* **2009**, *583*, 2419 – 2424; c) R. H. Schirmer, H. Adler, M. Pickhardt, E. Mandelkow, *Neurobiol. Aging* **2011**, *32*, 2325.
[35] L. E. Dietrich, T. K. Teal, A. Price-Whelan, D. K. Newman, *Science* **2008**, *321*, 1203 – 1206.
[36] a) M. Wainwright, K. Crossley, *J. Chemother.* **2002**, *14*, 431 – 443; b) F. R. Frankenburg, R. J. Baldessarini, *Harv. Rev. Psychiatry* **2008**, *16*, 299 – 307; c) M. Oz, D. E. Lorke, G. A. Petroianu, *Biochem. Pharmacol.* **2009**, *78*, 927 – 932.
[37] A. Küpfer, C. Aeschlimann, B. Wermuth, T. Cerny, *Lancet* **1994**, *343*, 763 – 764.
[38] C. M. Wischik, P. Bentham, D. J. Wischik, K. M. Seng, *Alzheimer's Dementia* **2008**, *4*, T167.
[39] T. Gura, *Nat. Med.* **2008**, *14*, 894.
[40] M. Necula, L. Breydo, S. Milton, R. Kayed, W. E. van der Veer, P. Tone, C. G. Glabe, *Biochemistry* **2007**, *46*, 8850 – 8860.
[41] S. Taniguchi, N. Suzuki, M. Masuda, S.-i. Hisanaga, T. Iwatsubo, M. Goedert, M. Hasegawa, *J. Biol. Chem.* **2005**, *280*, 7614 – 7623.
[42] J.-B. Wang, Y.-M. Wang, C.-M. Zeng, *Biochem. Biophys. Res. Commun.* **2011**, *415*, 675 – 679.
[43] E. Kachooei, A. A. Moosavi-Movahedi, F. Khodagholi, F. Mozaffarian, P. Sadeghi, H. Hadi-Alijanvand, A. Ghasemi, A. A. Saboury, M. Farhadi, N. Sheibani, *J. Biochem.* **2014**, *155*, 361 – 373.
[44] V. Banerjee, R. K. Kar, A. Datta, K. Parthasarathi, S. Chatterjee, K. P. Das, A. Bhunia, *PloS one* **2013**, *8*, e72318.
[45] M. Muzaffar, A. Ahmad, *PloS one* **2011**, *6*, e27906.
[46] A. Ahmad, I. S. Millett, S. Doniach, V. N. Uversky, A. L. Fink, *Biochemistry* **2003**, *42*, 11404 – 11416.
[47] A. Ahmad, I. S. Millett, S. Doniach, V. N. Uversky, A. L. Fink, *J. Biol. Chem.* **2004**, *279*, 14999 – 15013.
[48] J. Jana, R. K. Kar, A. Ghosh, A. Biswas, S. Ghosh, A. Bhunia, S. Chatterjee, *Mol. BioSys.* **2013**, *9*, 1833 – 1836.
[49] S. Ghosh, J. Jana, R. K. Kar, S. Chatterjee, D. Dasgupta, *Biochemistry* **2015**, *54*, 974 – 986.
[50] J. Bhat, S. Chatterjee, *RSC Adv.* **2016**, *6*, 36667 – 36680.
[51] D. R. Roe, T. E. Cheatham III, *J. Chem. Theory Comput.* **2013**, *9*, 3084 – 3095.
[52] S. S.-S. Wang, K.-N. Liu, T.-C. Han, *Biochim. Biophys. Acta, Mol. Basis Dis.* **2010**, *1802*, 519 – 530.
[53] S. Choudhary, N. Kishore, R. V. Hosur, *Sci. Rep.* **2015**, *5*, 17599.
[54] A. Ghosh, R. K. Kar, J. Jana, A. Saha, B. Jana, J. Krishnamoorthy, D. Kumar, S. Ghosh, S. Chatterjee, A. Bhunia, *ChemMedChem* **2014**, *9*, 2052 – 2058.
[55] S. Mondal, J. Jana, P. Sengupta, S. Jana, S. Chatterjee, *Mol. BioSys.* **2016**, *12*, 2506 – 2518.
[56] J. Wang, W. Wang, P. A. Kollman, D. A. Case, *J. Mol. Graphics Modell.* **2006**, *25*, 247 – 260.
[57] L. X. Dang, *J. Am. Chem. Soc.* **1995**, *117*, 6954 – 6960.
[58] Y. Shan, J. L. Klepeis, M. P. Eastwood, R. O. Dror, D. E. Shaw, *J. Chem. Phys.* **2005**, *122*, 054101.
[59] V. Kräutler, W. F. Van Gunsteren, P. H. Hünenberger, *J. Computat. Chem.* **2001**, *22*, 501 – 508.

Received: July 12, 2017
Revised manuscript received: August 24, 2017
Version of record online December 7, 2017

